Hydrogen partitioning behavior and related hydrogen embrittlement in Al-Zn-Mg alloys

Shimizu, Kazuyuki
Department of Mechanical Engineering, Kyushu University

Toda, Hiroyuki
Department of Mechanical Engineering, Kyushu University

Fujihara, Hiro
Department of Mechanical Engineering, Kyushu University

Hirayama, Kyosuke
Department of Mechanical Engineering, Kyushu University

他

出版情報：Engineering Fracture Mechanics. 216, pp.106503-, 2019-06. European Structural Integrity Society
バージョン：
権利関係：

Title:

Hydrogen partitioning behavior and related hydrogen embrittlement in Al-Zn-Mg alloys

Authors:

Kazuyuki Shimizu[*a], Hiroyuki Toda[a], Hiro Fujihara[a], Kyosuke Hirayama[a], Kentaro Uesugi[b], Akihisa Takeuchi[b],

Affiliations:

[a] Department of Mechanical Engineering, Kyushu University, Fukuoka, 819-0395, Japan

[b] Japan Synchrotron Radiation Research Institute, Hyogo, 679-5198, Japan

Corresponding author:

Name: Kazuyuki SHIMIZU

Affiliation: Department of Mechanical Engineering, Kyushu University, Motooka 744, Nishi-ku, Fukuoka-city, Fukuoka, 819-0395, Japan

Phone: +81-92-802-3300

E-mail: kshimizu@kyudai.jp

Abstract:

To develop high strength Al-Zn-Mg alloys, suppression of hydrogen embrittlement is indispensable. The hydrogen embrittlement behavior of different prepared Al-10.1-1.2Mg alloys with various hydrogen trap sites was observed using in situ synchrotron X-ray tomography in this study. Furthermore, we quantified the hydrogen partitioning based on hydrogen occupancies and hydrogen trap site densities in the prepared alloys. The combined analysis of hydrogen embrittlement and hydrogen partitioning showed that initial trapped hydrogen content in grain boundaries, vacancies, and dislocations before deformation was not crucial for inducing both intergranular fracture and quasi-cleavage fracture. However, hydrogen accumulates at grain boundaries and precipitate interfaces during deformation, inducing intergranular and quasi-cleavage fracture, respectively. Due to hydrogen accumulation, intergranular and quasi-cleavage fracture initiate when the hydrogen content at the grain boundary enriches 10^3~10^4 times the initial content and hydrogen content at the precipitate interface enriches 3.9×10^2 times the initial content, respectively. The change in hydrogen trap sites by processing and heat treatments did not suppress the intergranular and quasi-cleavage fracture. We conclude that generating new hydrogen trap sites (e.g., the interior of the intermetallic particle) in which hydrogen trap site density and binding energy are higher than the precipitate interface (> 33.87 kJ/mol) is beneficial to suppress hydrogen embrittlement.

Keywords: hydrogen embrittlement; Al-Zn-Mg alloy; hydrogen partitioning; intergranular fracture; quasi-cleavage fracture

1. Introduction

It has long been recognized that hydrogen in structural materials leads to the degradation of mechanical properties [1]. This phenomenon called hydrogen embrittlement (HE) has been extensively studied in materials such as steel [2,3], nickel alloys [4,5], and aluminum alloys [6,7]. The HE in aluminum alloys has not previously been regarded as important because of their low solubility in solid phase and the inability to form stable hydrides. However, in the case of high-strength Al-Zn-Mg alloys, it has been recognized that trace hydrogen leads to HE, degrading mechanical properties [7–9]. In other words, the suppression of HE is indispensable for developing high-strength aluminum alloys. The removal of hydrogen in an aluminum alloy by using particular casting processes or heat treatments in vacuum can improve mechanical properties [9,10], but it is not feasible in terms of manufacturing. To suppress HE, viable concepts for controlling hydrogen in aluminum alloys is needed.

Hydrogen is not uniformly present but is partitioned at different trap sites such as vacancies, dislocations, and grain boundaries, in aluminum alloys as shown in Eqs. (1) and (2) [11,12].

$$C_{\text{total}} = \theta_{\text{L}} N_{\text{L}} + \sum \theta_i N_i + C_{\text{pore}} \tag{1}$$

$$\frac{\theta_i}{1-\theta_i} = \theta_{\text{L}} \exp\left(\frac{E_i}{RT}\right) \tag{2}$$

where C_{total} is the total hydrogen content in an aluminum alloy and θ_{L} and θ_i are the occupancy of the interstitial and i-th trap site, respectively. N_{L} and N_i are the trap density in the normal interstitial lattice site and i-th trap site, respectively. C_{pore} is the total hydrogen content in the pores. The Eq. (2) express thermal equilibrium between interstitial hydrogen and hydrogen partitioned to trap sites [12]. E_i is the binding energy between hydrogen and the i-th trap site, R is the gas constant, and T is the temperature.

As shown in the Eqs. (1) and (2), hydrogen is partitioned in accordance with the trap site density and the occupancy derived by the binding energy at each trap site. To quantitatively evaluate the hydrogen partitioning in aluminum alloys, it is necessary to obtain the binding energy and the trap site density. The binding energy of each trap site in aluminum has been investigated by recent first-principles study (FPS), resulting 0.08 [13], 0.17 [13], 0.23~0.27 [14], 0.3 [15,16], 0.08~0.35 [17], and 0.7 [18] eV at screw dislocation, edge dislocation, high-energy grain boundaries, vacancy, precipitate interfaces, and surfaces, respectively. The trap site densities related to vacancy concentration, dislocation density and the surface area of grain boundary can be experimentally measured. Unlike binding energies, trap site densities can be increased or decreased by processing and heat treatments. For example, dislocation density increases after cold rolling. Heat treatments such as solution treatment and aging can change grain size and vacancy concentration. Changes in hydrogen trap sites affect hydrogen partitioning in aluminum alloys. In fact, it has been reported that a clear desorption peak from hydrogen trapped at dislocations was observed when a thermal desorption analysis of pure aluminum was performed after plastic deformation [19].

Representative fracture modes of HE in Al-Zn-Mg-Cu alloys are quasi-cleavage fracture and intergranular fracture [20]. It is understood that quasi-cleavage fracture and intergranular fracture are induced by the presence of hydrogen in dislocations/vacancies and grain boundaries, respectively [1]. Therefore, it is expected that HE can be suppressed without removing hydrogen by controlling trap site densities. This concept can be called hydrogen partitioning control. In the present study, we explore the concept of hydrogen partitioning control to suppress HE in Al-Zn-Mg alloys. First, Al-Zn-Mg alloys which have different trap site densities were prepared by the combination of heat treatments and rolling. Next, various experimental techniques such

as optical microscopy, modified Williamson-Hall method [21], and synchrotron X-ray tomography were applied to analyze both the trap site densities and the HE behavior of prepared alloys. Finally, the HE behavior of Al-Zn-Mg alloys is discussed from the aspects of hydrogen partitioning.

2. Methodology

2.1 Specimens

The materials used in this study were Al-10.1Zn-1.2Mg alloys in mass%. The Al-10.1Zn-1.2Mg alloys were, first, prepared by homogenization at 773 K for 7.2 ks after casting, hot rolling at 723 K with a rolling reduction of 50%. After that, six types of Al-10.1Zn-1.2Mg alloys with different grain size, dislocation density and vacancy concentration, which are hydrogen trap sites, were prepared by applying the process shown in Fig. 1. Alloys after solution treatment were quenched in ice water and immediately subjected to aging. The grain size was increased by increasing the time of solution treatments and the dislocation density was increased by an additional cold rolling of 50% as shown in Fig. 1. After performing additional rolling, an alloy having a high dislocation density and a low vacancy concentration was prepared by applying heat treatment at 423 K - 0.9 ks [22]. The fabrication of small tensile specimens and hydrogen charging were simultaneously performed by electrical discharge machining. The geometry of the small tensile specimen is the same as in the literature [7], and the gauge region is machined to a length of 0.7 mm and a cross-sectional area of 0.6×0.6 mm^2. By using vacuum fusion method, other authors have confirmed that the hydrogen content increases from 0.14 mass ppm to 6.97 mass ppm by EDM in water purified by ion exchange resins [9]. We also confirmed hydrogen content in prepared Al-Zn-Mg alloys after EDM cutting by a gas chromatography-type thermal desorption analyzer

(PDHA-1000, NISSHA FIS, Inc.). Analyzed total hydrogen content was 6.98 mass-ppm. This hydrogen content is same as the literature [9]. However, all hydrogen in the alloy did not desorb in one TDA analysis. More or less hydrogen remains after one TDA analysis. 10 consecutive TDA analysis after EDM cutting were performed, but all hydrogen was not desorbed. Approximately 0.1 mass ppm hydrogen is remained in a specimen after 10th TDA analysis. Therefore, we assumed total hydrogen content was equal to reference [9]. After EDM, the specimens have a high hydrogen content on their surface. To distribute hydrogen to the interior of the specimens, the specimens were stored in acetone for approximately four days. Assuming the diffusion coefficient of hydrogen in aluminum at room temperature is 2.3×10^{-11} m^2/s [19], the diffusion distance after four days is estimated to be 2.8 mm. This diffusion distance is more significant than specimen size, and hydrogen is assumed to diffuse from the surface to the center of the specimens.

To observe the morphology of grain in prepared alloys, 15 s chemical etching was carried out with a Keller's reagent after mirror polishing. After etching, the TD-ND plane (i.e., the plane where the rolling direction is normal direction) of the alloys was observed by an optical microscope, the mean equivalent diameter of grain was obtained.

2.2 Synchrotron X-ray imaging and in situ tests

In situ observations of HE behavior via synchrotron X-ray tomography were performed on BL20XU of SPring-8, Japan. The projection-type tomography was employed to observe the intergranular and quasi-cleavage cracking. The X-ray was monochromated by a Si(111) double-crystal monochromator, and the energy was tuned to 20 keV. The detector consisted of a 2048×2048 pixel CMOS camera, an optical lens,

and the single crystalline scintillator ($Lu_2Al_5O_{12}$:Ce). The distance between the specimen and the detector was 20 mm. The spatial resolution of this beamline is reported to be 1.2 μm [23]. Microstructural features such as pores and cracks exceeding this size were visualized in this study.

A small testing machine was installed on the rotation stage of the X-ray tomography system, and in situ observation of HE behavior was performed. In the tensile test, the initial strain rate was set at 3×10^{-3} s^{-1} by displacement control, and the test was performed at room temperature. This strain rate corresponded to the lowest setting of the in situ testing machine and it was measured from the tomographic images of tensile test-piece before and after loading. It was necessary to hold the displacement during tomography observation. A displacement of 0.02 mm, which is approximately 3% strain, was applied, and then the specimen was hold for 0.9 ks for tomographic observation. This sequence was repeated until the fracture of the specimen. The fracture surface was observed by a scanning electron microscope (SEM) after the tomographic experiments. A total of 1800 projection images were captured as the specimen was rotated by 180 degrees in steps of 0.1 degrees in tomographic observation, and these images were reconstructed into a 3D image by a filtered convolution backprojection algorithm [24].

Intergranular and quasi-cleavage cracks were extracted from 3D tomographic data and analyzed for morphology. All the pores in specimens were analyzed in 3D, and their gravity center, volume fraction, diameter, and surface area were calculated by the marching cubes algorithm [25].

3. Hydrogen embrittlement behavior

The HE behavior of the prepared Al-10.0Zn-1.2Mg alloys was examined. Fig.

2 shows nominal stress-nominal strain curves obtained by holding-time tests and Fig. 3 shows the fracture surface of their alloys after holding-time tests. Periodic stress drops in Fig. 2 is due to stress relaxation during tomographic scanning. The area fractions of intergranular fracture were calculated from Fig. 3 (a~f), and were 22%, 71%, 96%, 8%, 10%, and 73%, respectively. The area fractions of quasi-cleavage fracture also were calculated from Fig. 3 (a~f), and were 4%, 29%, 4%, 32%, 42%, and 3%, respectively. As shown in Fig. 2 (a), the fracture strain increased with shorter times of solution treatment. A microstructural feature which varies solution treatment time is the grain size. Grain sizes at solution treatment times of 0.12, 1.2, and 120 ks were 98, 259, and 678 μm, respectively. From Figs. 2 and 3, it is found that the larger the grain size, the smaller both fracture strain and the tendency to induce intergranular fracture. Besides, the nominal stress remarkably decreased at the nominal strain of 11% in the alloy which solution treatment time is 120 ks. This is presumed to be due to crack propagation while holding displacement in tomographic observation. Crack propagation under fixed-displacement during tomographic scanning was also observed in the previous study [26], and the propagation path was along the grain boundaries. As a result, it has been suggested that hydrogen accumulation in grain boundaries decrease the local crack resistance.

We evaluate the influence of initial vacancy concentration on HE behavior by comparing annealed and non-annealed alloys. This corresponds to the comparison of the black line and the red line in Fig. 2, and of their fracture surface shown in Fig. 3 (d) and (e). It can be seen that the flow stress and the fracture strain decrease in the alloy with high vacancy concentration in Fig. 2 (b). In the fracture surfaces shown in Fig. 3 (d) and (e), significant differences in the area fractions of both intergranular fracture and quasi-cleavage fracture are not recognized. The reason for premature fracture in an

alloy with a high vacancy concentration is due to the occurrence of longitudinal cracks, in which intergranular cracks propagate parallel to the loading direction, as shown by the broken line region in Fig. 3 (d). Longitudinal cracks initiate along specific grain boundaries which is affected by complex triaxial stress state in the necked region [27,28]. Therefore, it can be considered the initial vacancy concentration before tensile loading has little influence on both intergranular fracture and quasi-cleavage fracture in prepared alloys.

We compare HE behavior with respect to dislocation density. As it can be seen from (d) and (e) in Fig. 3, quasi-cleavage fracture tends to initiate easily in alloys which have high dislocation density by additional cold rolling. The area fraction of quasi-cleavage fracture in Fig. 3 (e) was 42%. However, its fracture behavior is not completely brittle, exhibiting undulated and tortures morphology on the quasi-cleavage facet in Fig. 3 (e). In addition, its fracture strain was 39%, as shown in the black line of Fig. 2 (b). These results imply that quasi-cleavage cracks were propagating and meandering accompanying plasticity during loading.

In-situ observation of the morphology of intergranular and quasi-cleavage cracks during deformation of prepared alloys by X-ray microtomography was performed. As a representative example, the visualization of cracks in an alloy with a solution treatment time of 1.2 ks is shown in Fig. 4. The fracture surfaces observed by SEM indicated in Fig. 4 (a-c) are the same as Fig. 3 (b). The visualized cracks at the strain of 11.8%, and 30.5% are superimposed with yellow on fracture surface in Fig. 4 (b) and Fig. 4(c), respectively. Intergranular cracks, especially located at the upper and the right side in Fig. 4 (b), were initiated from the surface of an alloy, gradually propagate, and transform to quasi-cleavage cracks with an increase in the distance from the surface to the center of the specimen. Intergranular and quasi-cleavage cracks are

usually categorized into brittle crack [1], but they did not propagate instantaneously on one-grain boundary plane or one facet. Both cracks propagated gradually in response to tensile load.

4. Analysis of H partitioning behavior

In this chapter, the HE behavior mentioned in chapter 3 will be evaluated in terms of hydrogen partitioning. As stated in the introduction, the hydrogen partitioning in aluminum is represented by the trap site densities and occupancies of hydrogen according to Eq. (1). The hydrogen partitioning of prepared alloys before deformation was calculated based on their occupancies and trap site densities. Chapter 4 details the quantitative analysis of the hydrogen trap site and hydrogen occupancy, and then, evaluates the HE behavior based on hydrogen partitioning.

In the hydrogen partitioning calculation based on the Eq. (1), the total hydrogen content of prepared alloys was set to 6.97 mass ppm [9]. The mechanism of hydrogen charging by EDM in purified water is recognized to be following surface reaction: $2Al + 3H_2O \rightarrow Al_2O_3 + 6H$ [29]. This reaction is a simple surface reaction and the effect of trap site changes in prepared alloys on this reaction is considered to be small. Therefore, it was assumed that the total hydrogen content in prepared alloys do not change.

4.1 Evaluation of hydrogen trap-site densities

Hydrogen trap sites in Al-Zn-Mg alloys used in this study are grain boundaries, dislocations, pores, vacancies, precipitate interfaces. In order to quantitatively analyze these trap site densities, the area of grain boundary, dislocation density, pore morphology, vacancy concentration, and the area of precipitate interface were obtained

by some experimental techniques and mathematical models that will be explained in this section. Quantified microstructural features in prepared alloys were summarized in Table 1. The details are described below.

Regarding the grain boundary area, the total grain boundary areas per unit aluminum volume were calculated based on the grain size. The grain size increased from 98 μm to 678 μm due to the increase in solution treatment time, and the grain size decreased from 372 μm to 273 - 284 μm by additional cold rolling, as shown in Table 1.

Dislocation density was analyzed using modified Williamson-Hall method [21], and some parameters which necessary for this calculation were referred to the literature [30]. As the results, calculated dislocation densities of prepared alloys were 3.45×10^{14}, 5.47×10^{14}, 3.09×10^{14}, and 4.67×10^{14} m^{-2} for the alloys with solution treatment times of 0.12, 1.2, 120 and 7.2 ks, respectively. The dislocation densities of the high C_v - high $\rho_{disl.}$ alloy and the low C_v - high $\rho_{disl.}$ alloy in Fig. 2 is 8.15×10^{15} and 9.06×10^{15}, m^{-2} respectively. These results show that the dislocation density was increased by approximately one order of magnitude when 50% additional cold rolling was applied.

The morphology of pores was visualized in three-dimensions by synchrotron X-ray tomography. The volume and surface area of all the pores present in the gauge region of prepared alloys were analyzed by the marching cubes algorithm [25]. In the process of Fig. 2, processes which affect the morphology of pores are solution treatment and additional rolling. As can be seen from Table 1, the volume fraction and diameter of the pores increased with increasing solution treatment time due to the growth of pores by holding at high temperature. In contrast, the volume fraction and the mean diameter of pores decreased in high C_v - high $\rho_{disl.}$ alloy and the low C_v - high $\rho_{disl.}$ alloy because

pores were annihilated or shrunk by additional rolling.

When estimating the hydrogen present in the pores, it is necessary to calculate the molecular hydrogen content inside the pores, $C_{\mathrm{H_2}}$[11], in addition to the adsorbed hydrogen at the surface of pores, $C_{\mathrm{ads.H}}$ [18], described by the trap site density and occupancy as with other trap sites. Trapped hydrogen content in the pores, C_{pore}, is expressed as:

$$C_{\mathrm{pore}} = C_{\mathrm{ads.H}} + C_{\mathrm{H_2}} = \theta_s N_s + 2N_A \frac{4\gamma V_{\mathrm{pore}}}{d_{\mathrm{pore}} RT} \tag{3}$$

where θ_s and N_s are the occupancy and the trap site density of adsorbed hydrogen in pores, respectively, N_A is the Avogadro's constant, V_{pore} and d_{pore} are the total volume of pores in unit aluminum volume and the mean diameter of pores, respectively, R is the gas constant, T is the temperature. γ is the surface energy of aluminum. Molecular hydrogen content in pores, $C_{\mathrm{H_2}}$, is expressed by energy balance between the surface energy of the aluminum matrix and the internal gas pressure of pores in Eq. (3) [11]. The surface energy of materials is decreased by the adsorbed hydrogen at the surface and is expressed as [18,31]:

$$\gamma = \gamma_0 - \left(E_S + RT\ln(\theta_L)\right)\frac{N_S\theta_S}{N_A A_{\mathrm{pore}}} + \frac{N_s}{N_A A_{\mathrm{pore}}} RT\{\theta_s \ln(\theta_s) + (1-\theta_s)\ln(1-\theta_s)\} \tag{4}$$

where γ_0 is the initial surface energy (1 J/m^2) [14,18], E_s is the binding energy of adsorbed hydrogen at the surface of pores, A_{pore} is the total surface area of pores in unit aluminum volume.

The vacancy concentration of the alloys not subjected to additional rolling was calculated by a thermal equilibrium model given by the following Eq. [32]:

$$C_{\mathrm{v}} = 3.19 \exp\left(-\frac{Q_{\mathrm{f}}}{k_{\mathrm{B}} T}\right) \tag{5}$$

where Q_{f} is the formation energy of vacancy equal to 0.55 eV [15] and k_{B} is the

Boltzmann's constant. For the vacancy concentration of prepared alloys subjected to additional rolling, the vacancies formed during rolling were taken into consideration. Militzer *et al.* documented that the vacancy formation rate under external loading is expressed as [33]:

$$\frac{\mathrm{d}C_\mathrm{v}}{\mathrm{d}t} = \chi\frac{\Omega_0\sigma}{Q_\mathrm{f}}\dot{\varepsilon} + \zeta\frac{C_\mathrm{j}\Omega_0}{4b^3}\dot{\varepsilon} - \frac{D_\mathrm{v}\rho}{\kappa^2}c_\mathrm{v} - \frac{D_\mathrm{v}}{L^2}c_\mathrm{v} \quad (6)$$

where χ = 0.1 is the dimensionless constant [33], σ is the flow stress, Ω_0 is the atomic volume, $\dot{\varepsilon}$ is the strain rate, b is Burgers vector, ζ describes the neutralization effect induced by the presence of vacancy emitting and vacancy absorbing jogs, C_j is the concentration of thermal jogs, D_v is the vacancy diffusivity, ρ is the dislocation density, L is the grain size, κ=1 is a parameter expressing the distribution of dislocations [33,34]. Witzel proposed that the second term in Eq. (6) is only applied in the temperature range over 0.4 of the melting temperature [33,35]; therefore, the second term is not considered in this study. The third and fourth terms of Eq. (6) are related to the annihilation of vacancies during deformation and are described as a function of vacancy concentration and dislocation density during deformation. It is complicated to estimate the vacancy concentration and dislocation density during rolling in this study. In addition, Deschamps *et al*. have reported that the terms of the annihilation of vacancies, which correspond to the third and the fourth term in Eq. (6), are much smaller than the first term describing vacancy formation [34]. Therefore, vacancy annihilation was not taken into the calculation of vacancy concentration after the cold rolling in this study, but only the formation of vacancies was considered. It is given by the integral of the simplified Eq. (6) as follows:

$$C_\mathrm{v} = \chi\frac{\sigma\Omega_0}{Q_\mathrm{f}}\varepsilon + C_0 \quad (7)$$

where ε is the strain, C_0 is the initial vacancy concentration calculated by Eq. (5). As mentioned above, the vacancy concentration obtained by Eq. (7) is estimated as the upper limit of the vacancy concentration after rolling because the annihilation process is not taken into consideration.

The area of the precipitate interface was calculated from the result of TEM observation. According to Bend *et al.*, The primary precipitate of the prepared alloys is specified η_2 [36–38]. The habit plane of η_2 is $\{111\}_{Al}$ and its morphology is disk-like [37]. The diameter of the plate plane and the length of the end plane of the observed η_2 precipitate were approximately 20 nm and 5 nm, respectively. Even though aging condition is overaging, the plate plane of η_2 precipitate was coherent with the aluminum matrix. On the other hand, interfacial structure between the end plane of η_2 precipitate and the aluminum matrix has been reported semi-coherent, that is, the existence of interfacial dislocations. A principal plane in terms of hydrogen trap in Al-Zn-Mg alloys is the coherent interface of disk-shaped precipitates. Tsuru *et al.* have clarified that the coherent interface of η_2 is one of the hydrogen trap sites by FPS [17]. This trap site density of the precipitate was determined from the number density of the precipitates, assuming the thickness of the TEM specimen to be 50 nm. The number density of the precipitates was 1.35×10^{23} m^{-3}.

Considering the result of Table 1 and the hydrogen trap interval of each trap site calculated by FPS, the trap site densities of hydrogen, N_i, in Eq. (1) were derived and used for hydrogen distribution calculation. This hydrogen trap interval is corresponding to the maximum density at which hydrogen can present in each trap site, i.e., trapped hydrogen content when the occupancy is equal to 1. These are 22 atomH/nm^2 for the grain boundary [14], 2.8 atomH/nm for the edge dislocation [13], 3.2 atomH/nm for the screw dislocation [13], 8 atomH/vacancy for the vacancy [16],

6.1 atomH/nm^2 for the coherent interface of precipitate [17], 20 atomH/nm^2 for the pore [18].

4.2 Evaluation of hydrogen occupancies

As mentioned in the introduction, the hydrogen occupancy of each site is described by the thermal equilibrium of occupancies between interstitial hydrogen and hydrogen at each trap site, as described in Eq. (2). In the calculation of Eq. (2), binding energies, E_i, revealed by FPS were used and are summarized in Table 2. Trapping sites that showed the lowest and the highest binding energy were the screw dislocation and the surface of pore, respectively.

Binding energy can also be evaluated experimentally employing thermal desorption analysis [19,39]. In thermal desorption analysis, the energy that hydrogen desorbs from the trap site (i.e., desorption energy) can be measured, and then, the binding energy can be obtained by subtracting the activation energy of the lattice diffusion of hydrogen from the desorption energy. However, the trap site in an aluminum alloy changes from the relatively early stage of temperature raising. For example, the vacancy concentration increases exponentially with temperature rise as shown in Eq. (4), and are 1.85×10^{-9} at 300 K and 3.77×10^{-7} at 400 K. The morphology of the precipitate also changes significantly around aging temperature (~ 473 K). The temperature at which both trap sites change and hydrogen desorption from trap sites are overlapped, leading a difficulty to measure the binding energy. Ebihara *et al.* have reported the numerical simulation of thermal desorption analysis incorporating trap site changes during heating [40]. The calculated binding energy of dislocations in aluminum increases from 16.4 kJ/mol to 27.6 kJ/mol due to changes in dislocation density during temperature rise in their study. Based on the above reasons, precise experimental

evaluation of the binding energy of hydrogen in aluminum was infeasible, and therefore FPS was utilized as a helpful alternative.

4.3 Hydrogen partitioning behavior and related hydrogen embrittlement

Fig. 5 shows the results of the hydrogen partitioning calculation of the six types of prepared alloys. The magnitude of the occupancy for each trap site is shown in Fig. 5 (a) an it exponentially depended on the magnitude of the binding energy. As with binding energy, the occupancy of hydrogen trap sites was the highest in pores and the lowest in dislocations. Focusing on one trap site, it is found that even if the trap site is changed by processing or heat treatment, the occupancy does not fluctuate significantly. Fig. 5 (b) is the summary of the hydrogen content of each trap site. The trapped hydrogen content, C_i, is represented by the product of occupancy, θ_i, and the trap site density N_i. The trap site with the highest occupancy was pore, but the trapped hydrogen content was the maximum at the precipitate interface. This is caused by a difference in trap site densities. The dispersion interval the pores in the matrix is on the order of several to several tens of μm, and that of the precipitates is several nm. The trap site density of precipitates is larger than that of pores.

HE, i.e., intergranular and quasi-cleavage fracture are discussed from the viewpoint of hydrogen partitioning shown in Fig. 5. First, we focus on the intergranular fracture. Fig. 6 shows the relationship between the area fraction of intergranular fracture calculated from Fig.3 and the trapped hydrogen content in grain boundaries extracted from Fig. 5(b). There was no correlation between the trapped hydrogen content in the grain boundaries and the area fraction of intergranular fracture. In the calculation of hydrogen partitioning at grain boundaries, the effect of grain size is reflected as the trap site density of grain boundaries. As the grain size decreases, the total area of grain

boundaries per 1 m^3 of aluminum increases and the trapped hydrogen content in the grain boundaries increases. For instance, when solution treatment times are 0.12, 1.2, and 120 ks, the grain sizes are 98, 259, and 678 μm (Table 1), trapped hydrogen contents in the grain boundary are 1.6×10^{19}, 7.1×10^{18}, and 2.3×10^{18} atomH/m^3 (Fig. 5(b)), and the area fractions of intergranular fracture were 22%, 71% and 96%, respectively. Comparison of these three alloys shows that the higher trapped hydrogen content in grain boundaries, the less intergranular fracture occurs, which is unrealistic interpretation. The result of Fig. 6 means that the trapped hydrogen content in the grain boundaries before deformation is not the dominant factor of the intergranular fracture of prepared alloys. From Fig. 5 (b), it is found that the trapped hydrogen content in the grain boundaries is remarkably lower than other trap sites. In order to increase the trapped hydrogen content in the grain boundaries to the level at which grain boundary decohesion occurs, hydrogen accumulation in the grain boundaries during deformation is indispensable. The authors have reported the influence of holding-times on the intergranular fracture of the low C_v - low $\rho_{disl.}$ Alloy [26]. As the results, at holding times of 0.3, 0.9, and 2.7 ks, the area fractions of intergranular fracture were 19%, 58%, and 61%, respectively [26]. The strain rate in this experiment was 3.0×10^{-3} s^{-1}, the same as in this study. It is considered that decrease in hydrogen content in alloys with the increase of holding-time is slight because aluminum has passive oxide on the surface. It has been clarified that as the holding-time increases, the area fraction of intergranular fracture increases. This mechanism is considered as follows. A strain field and a hydrostatic stress field are formed ahead of the crack tip, and it has been reported that hydrogen is accumulated there [41,42]. An increase in holding-time corresponds to an increase in the accumulation time of hydrogen at the crack tip, resulting in an increase in local hydrogen content near the crack tip. Initial crack after applying loading in low

C_v - low $\rho_{disl.}$ Alloys was intergranular crack. Naturally, the tip of the intergranular crack is a grain boundary, and hydrogen accumulates at this grain boundary. As will be described later, an increase in hydrogen content at grain boundaries results in a decrease in grain boundary cohesive energy, i.e., a decrease in local crack resistance [14]. This is considered to have appeared as an increase in the area fraction of intergranular fracture in the observation of fracture surface in the literature [26]. The relationship between grain boundary decohesion and hydrogen accumulation was also approached from FPS. Yamaguchi *et al.* revealed that grain boundary approaches zero and grain boundary decohesion occurs when trapped hydrogen in Σ5(012) grain boundary of aluminum reaches approximately 20 atomH/nm^2 [14]. When this amount of trapped hydrogen in grain boundaries is applied to alloys used in this study and is converted to the trapped hydrogen content in the grain boundaries in unit aluminum volume, it becomes approximately 2×10^{22} atomH/m^3. The trapped hydrogen content in the grain boundaries shown in Fig. 5(b) are $2.3\times10^{18} \sim 1.6\times10^{19}$ atomH/m^3, and in order to satisfy the intergranular fracture criterion led by Yamaguchi *et al*., the trapped hydrogen content in grain boundaries needs to be 10^3~10^4 times higher than that of before deformation [14]. Regarding this unrealistic magnitude of hydrogen enrichment, Yamaguchi *et al.* also mentioned it in their report [14].

This fracture criterion describes the state where the intergranular fracture occurs only by hydrogen accumulation, and the distribution of mechanical stress/strain on the grain boundary is not considered. In actual intergranular fracture, it is considered that this decrease in cohesive energy by hydrogen accumulation and the stress/strain localization on the grain boundary simultaneously work, inducing intergranular fracture. This indirect basis for this is shown in Fig 7. It can be seen from Fig. 7, there is a weak correlation between the area fraction of intergranular fracture and grain size. The grain

size of the prepared alloys is on the order of several hundreds of μm, which is coarse as compared to the practical alloys (several tens of μm). It is inferred that deformation near the grain boundary of prepared alloys are heterogeneous because the number of adjacent grains is small, and the plastic constraint is low. In the deformation behavior near grain boundaries, both dislocation pile-up at grain boundaries and dislocation transport to grain boundaries occur. This appears as localization of strain near grain boundaries. Toda *et al.* experimentally visualized that 3D/4D plastic strain distribution in the vicinity of grain boundaries in an aluminum alloy by a synchrotron imaging technique, namely diffraction-amalgamated grain boundary tracking [43]. They revealed that plastic strain distribution in the grain boundaries is localized and is complicated due to cooperative deformation by the plurality of grains. Contos and Starke examined slip planarity and related fracture behavior in aluminum alloys by atomic force microscopy [44]. They concluded that strain localization and stress concentrations on grain boundaries promote intergranular fracture. Thus, it is considered that intergranular fracture is affected not only by the local hydrogen content in the grain boundaries but also by heterogeneous deformation near the grain boundary.

Next, we focus on the quasi-cleavage fracture from the viewpoint of hydrogen partitioning. Regarding the mechanism of quasi-cleavage fracture, as well as intergranular fracture, much discussion has been made such as nanovoid coalescence [45], dislocation process [46,47], and the combination of dislocation nucleation and mobility [48] under hydrogen influence. Many of them include interaction among vacancies, dislocations, and hydrogen. Fig. 8 shows the relationship between the area fraction of quasi-cleavage fracture calculated from the fracture surface of Fig. 3 and the trapped hydrogen content in vacancies and dislocations. There is no correlation between the area fraction of the quasi-cleavage fracture and the trapped hydrogen content in

vacancies, and it seems that there is a weak correlation in the trapped hydrogen content in dislocations. However, the trapped hydrogen content in dislocations is not the factor of the quasi-cleavage fracture. As can be seen from Fig. 5 (b), the trapped hydrogen content in dislocations is lower than pores, precipitates, and the vacancies after rolling, and the occupancy is the lowest among trap sites. The occupancy of dislocations was 2.7×10^{-5} on average. Because the trap hydrogen density of the dislocation when occupancy equal to 1 is 3 atomH/nm, 8.1×10^{-5} hydrogen atoms are present on 1 nm of dislocation line in prepared alloys. It is difficult to consider that this low-density hydrogen atoms on the dislocation line is the origin of quasi-cleavage fracture. Unlike grain boundaries, hydrogen accumulation cannot be expected in dislocations in aluminum. The findings related to hydrogen accumulation in dislocations is limited, and the simulation of tungsten with the high binding energy of dislocation has been reported [49]. The interactions between the hydrogen and the dislocations, which are not hydrogen accumulation into dislocations, have been investigated by many researchers. Examples include an increase in mobility of dislocation by hydrogen [4] and hydrogen transport by dislocation [50,51]. The present study does not controvert these interactions between dislocations and hydrogen. Hydrogen transport by dislocation is also experimentally observed in aluminum alloys [52,53], and it is also clarified that the internal equivalent strain in Al-Zn-Mg-Cu alloys is localized by hydrogen [7,9]. However, we consider that trapped hydrogen in dislocations is not the origin of quasi-cleavage fracture due to the lowest occupancy in prepared alloys described above.

From Fig. 5 (b), the site trapping the most hydrogen is the precipitate interface. The finding that precipitates trap hydrogen is reported not only in aluminum but also in steel. Nagao *et al.* reported that interfacial decohesion of precipitates induce quasi-

cleavage fracture in steel [54,55]. However, hydrogen-induced precipitate decohesion or the hydrogen-induced quasi-cleavage cracks along the (Ti, Mo)C precipitate/matrix interface were not observed in their study. Furthermore, the binding energy is larger at the high-angle grain boundary (57.4 kJ/mol) than (Ti, Mo)C precipitate (30.5 kJ/mol) [56]. The unclear point in their study, which is from standpoints of hydrogen partitioning, is that why quasi-cleavage cracks along the precipitate/matrix interface and lath boundaries rather than intergranular crack dominate the hydrogen-induced fracture. Al-Zn-Mg alloys do not have a lath structure like steels the above described. Therefore, even simply called quasi-cleavage fracture, it might be different from that of steels. Tsuru *et al.* clarified the hydrogen trap in the precipitate interface of $MgZn_2$ in aluminum [17], which is reflected in the calculation of Fig. 5 as the parameters of hydrogen partitioning. Furthermore, Tsuru *et al.* have revealed that the interfacial decohesion of precipitates initiate when the trapped hydrogen density reaches 18.9 atomH/nm^2 due to hydrogen accumulation by FPS [57]. No mechanical load and no interfacial dislocation are given in this calculation. It is clarified that interfacial decohesion is caused simply by hydrogen accumulation at the interface of $MgZn_2$/Al. Even if the occurrence of interfacial dislocations or dislocation pile-up at the precipitate interface, the hydrogen binding energy of dislocations is low (Table 2), therefore, these influence on hydrogen accumulation in the precipitate is quite limited. The trapped hydrogen density in the precipitate interface of prepared alloys is approximately 4.8×10^{-2} atomH/nm^2 from the occupancy of the precipitate interface in Fig. 5 (a). Therefore, if 3.9×10^2 times hydrogen concentration in the precipitate interfaces occurs locally during deformation, initiating cracks due to interfacial decohesion of precipitates. When hydrogen accumulates in the local region during deformation, the hydrogen repartitioning within that region depends on the binding energy. Although the

trap site having the highest binding energy is pores as shown in Table 2, hydrogen accumulation in pores during deformation is quite limited because the occupancy of pores is almost 1 before deformation as shown in Fig. 5(a). The trap site having the second highest binding energy is the precipitate interface (33.87 kJ/mol at the MgZn-mixed interface of precipitate). Because the occupancy of hydrogen in the precipitate interface before deformation is still 7.8×10^{-3}, an increase in occupancy due to hydrogen accumulation can be expected. Considering that the precipitate interface is a very limited region (20 nm in diameter) and is one of the singular stress fields, the probability of hydrogen enrichment of 3.9×10^{2} times is conceivable. Furthermore, the source of hydrogen that accumulates at this interface can be either hydrogen repartitioning inside an alloy or hydrogen penetration from the outside of an alloy. The influence of external hydrogen is not taken into consideration in the hydrogen partitioning calculation of this study. In environments where hydrogen can penetrate from the outside such as humid air, the above decohesion criterion will be more likely to be satisfied because local hydrogen content is expected to increase [29].

These precipitates are aligned precipitates arranged on the {111} plane in grain interior [37]. Assuming quasi-cleavage fracture occurs due to interfacial decohesion of precipitates by hydrogen accumulation, the crystallographic orientation of the quasi-cleavage facet might {111} plane. Hirayama *et al.* investigated the crystallographic orientation of the quasi-cleavage facet in an Al-Zn-Mg alloy, which is the same alloy in this study, by diffraction contrast tomography [58]. They revealed that there is no specific orientation relationship between the quasi-cleavage facet and the crystallographic plane of the matrix. As mentioned in Chapter 3, the quasi-cleavage fracture behavior of prepared alloys is not completely brittle and involves plasticity, leading undulated quasi-cleavage facets shown in Fig. 3. We will integrate both the

results of the present study and Hirayama *et al.* and discuss the process of quasi-cleavage fracture. First, the precipitate interface satisfying the decohesion criterion by hydrogen accumulation is cracked during deformation. We consider that this might be the origin of quasi-cleavage crack. Next, the quasi-cleavage crack propagates along the above-cracked precipitate interface. The crack path on {111} interface is not necessary on the identical crystallographic plane. The aluminum matrix has four equivalent {111} planes, of which crack propagates selectively in the precipitate/aluminum interface where hydrogen accumulation is remarkable. It is considered that the contribution of both plastic deformation and hydrogen accumulation overlapped on the quasi-cleavage crack propagation, exhibited a complicated facet morphology.

Finally, we consider what kind of microstructural control is useful for suppressing HE. The present study shows that HE, especially quasi-cleavage fracture cannot be suppressed even if the grain size, dislocation density, and vacancy concentration are changed by processing. To suppress quasi-cleavage fracture, it is necessary to reduce the hydrogen partitioned to the precipitate interface. For that purpose, it is helpful to partition hydrogen to the site which has higher binding energy and trap site density than precipitates. Specific candidates for the trap site include the interior of the intermetallic particles. Practical aluminum alloys contain impurities such as iron and silicon, forming micron-sized intermetallic particles such as Al_7Cu_2Fe and Mg_2Si [59]. According to Su *et al.*, increasing the volume fraction of intermetallic particles by enriching both Fe and Si content from 0.01 to 0.30 mass% suppressed the area fraction of the quasi-cleavage fracture from 22.4% to 8.1% in Al-Zn-Mg-Cu alloys [60]. Given that hydrogen is trapped inside the intermetallic particles and the trapped hydrogen content in the precipitate interfaces is lowered, suppression of quasi-cleavage fracture can be interpreted. The application of intermetallic particles as a favorable

hydrogen trap sites which suppress HE is beneficial in both academic and industrial fields. However, the hydrogen trap inside intermetallic particles is no more than a hypothesis. In addition, Su *et al.* have evaluated the suppression of hydrogen embrittlement by intermetallic particles using hydrogen pre-charged alloys in the above literature. Intermetallic particles can trap a limited amount of hydrogen. When hydrogen trapping sites in the intermetallic particles are occupied by hydrogen in an environment where hydrogen is continuously supplied from outside the specimen, there is a high possibility that the suppression of hydrogen embrittlement by the intermetallic particles is not effective. In the future works, it will be necessary to quantitatively analyze the suppression effect of quasi-cleavage fracture by intermetallic particles from the aspects of hydrogen partitioning.

5. Conclusions

Al-10.1Zn-1.2 Mg alloys with different hydrogen trap sites were prepared by the combination of heat treatment and rolling, and their HE behavior was investigated. The calculation of hydrogen partitioning was carried out based on the binding energies of hydrogen derived by FPS and the trap site densities of hydrogen obtained by various analysis and related HE behavior was quantitatively evaluated. Regarding intergranular fracture, there was no correlation with initial trapped hydrogen content in the grain boundaries before deformation. Hydrogen partitioning calculation revealed that the criterion for intergranular fracture derived by the FPS is satisfied when the trapped hydrogen content in the grain boundaries increases locally by 10^3~10^4 times as compared to the initial content. In addition, heterogeneous deformation depending on grain size affected intergranular fracture. The mechanism of quasi-cleavage fracture could not be interpreted based on trapped hydrogen content in vacancies and

dislocations. The site which traps the most hydrogen in the Al-10.1Zn-1.2Mg alloys was the precipitate interface. It has been calculated that hydrogen accumulates at the interface of this precipitate during deformation, and the interfacial decohesion of precipitates occurs when the trapped hydrogen content increases to 4.9×10^2 times of initial content.

Acknowledgments

This research was supported by Japan Science and Technology Agency (JST) under Collaborative Research Based on Industrial Demand "Heterogeneous Structure Control: Towards Innovative Development of Metallic Structural Materials", Grant Number JPMJSK1412, Japan. This research was supported in part by a grant from the Light Metal Educational Foundation, Japan. The synchrotron radiation experiments were performed at the BL20XU of SPring-8 with the approval of Japan Synchrotron Radiation Research Institute (JASRI) (Proposal No. 2017A0076, 2017B0076).

Reference

[1] Robertson IM, Sofronis P, Nagao A, Martin ML, Wang S, Gross DW, et al. Hydrogen Embrittlement Understood. Metall Mater Trans A Phys Metall Mater Sci 2015;46:2323–41. doi:10.1007/s11661-015-2836-1.

[2] Beachem CD. A new model for hydrogen-assisted cracking (hydrogen "embrittlement"). Metall Trans 1972;3:441–55. doi:10.1007/BF02642048.

[3] Koyama M, Rohwerder M, Cem Tasan C, Bashir A, Akiyama E, Takai K, et al. Recent progress in microstructural hydrogen mapping in steels: quantification, kinetic analysis, and multi-scale characterisation. Mater Sci Technol 2017;33:1481–96. doi:10.1080/02670836.2017.1299276.

[4] Birnbaum HK, Sofronis P. Hydrogen enhanced localized plasticity—A mechanism for hydrogen related fracture. Mater Sci Eng A 1994;176:191–202.

[5] Martin ML, Somerday BP, Ritchie RO, Sofronis P, Robertson IM. Hydrogen-induced intergranular failure in nickel revisited. Acta Mater 2012;60:2739–45. doi:10.1016/j.actamat.2012.01.040.

[6] Lynch SP. Environmentally assisted cracking: Overview of evidence for an adsorption-induced localised-slip process. Acta Metall 1988;36:2639–61. doi:10.1016/0001-6160(88)90113-7.

[7] Su H, Toda H, Masunaga R, Shimizu K, Gao H, Sasaki K, et al. Influence of hydrogen on strain localization and fracture behavior in Al-Zn-Mg-Cu aluminum alloys. Acta Mater 2018;159:332–43. doi:10.1016/J.ACTAMAT.2018.08.024.

[8] Christodoulou L, Flower HM. Hydrogen embrittlement and trapping in Al-6%Zn-3%Mg. Acta Metall 1980;28:481–7. doi:10.1016/0001-6160(80)90138-8.

[9] Bhuiyan MS, Tada Y, Toda H, Hang S, Uesugi K, Takeuchi A, et al. Influences of hydrogen on deformation and fracture behaviors of high Zn 7XXX aluminum alloys. Int J Fract 2016;200:13–29. doi:10.1007/s10704-016-0092-z.

[10] Toda H, Oogo H, Horikawa K, Uesugi K, Takeuchi A, Suzuki Y, et al. The true origin of ductile fracture in aluminum alloys. Metall Mater Trans A Phys Metall Mater Sci 2014;45:765–76. doi:10.1007/s11661-013-2013-3.

[11] Toda H, Hidaka T, Kobayashi M, Uesugi K, Takeuchi A, Horikawa K. Growth behavior of hydrogen micropores in aluminum alloys during high-temperature exposure. Acta Mater 2009;57:2277–90. doi:10.1016/j.actamat.2009.01.026.

[12] Oriani RA. The diffusion and trapping of hydrogen in steel. Acta Metall 1970;18:147–57. doi:10.1016/0001-6160(70)90078-7.

[13] Itakura M, Yamguchi M, Ebihara K, Matsuda K, Toda H. First-principles calculations of hydrogen trapping energy at screw and edge dislocations of aluminum. in preparation.

[14] Yamaguchi M, Ebihara K-I, Itakura M, Tsuru T, Matsuda K, Toda H. First-principles calculation of multiple hydrogen segregation along aluminum grain boundaries. Comput Mater Sci 2019;156:368–75. doi:10.1016/j.commatsci.2018.10.015.

[15] Enomoto T, Matsumoto R, Taketomi S, Miyazaki N. First-principles estimation of hydrogen occupancy around lattice defects in Al. Zair Soc Mater Sci Japan 2010;59:596–603. doi:10.2472/jsms.59.596.

[16] Ismer L, Park MS, Janotti A, Van De Walle CG. Erratum: Interactions between hydrogen impurities and vacancies in Mg and Al: A comparative analysis based on density functional theory (Phys. Rev. B (2009) 80 (184110)). Phys Rev B - Condens Matter Mater Phys 2010;81:184110. doi:10.1103/PhysRevB.81.139902.

[17] Tsuru T, Yamaguchi M, Ebihara K, Itakura M, Shiihara Y, Matsuda K, et al. First-principles study of hydrogen segregation at the MgZn2 precipitate in Al-Mg-Zn alloys. Comput Mater Sci 2018;148:301–6. doi:10.1016/j.commatsci.2018.03.009.

[18] Yamaguchi M, Tsuru T, Ebihara K, Itakura M. Surface energy reduction by dissociative hydrogen adsorption on inner surface of pore in aluminum. J Japan Inst Light Met 2018;68:588–95. doi:10.2464/jilm.68.588.

[19] Young GA, Scully JR. The diffusion and trapping of hydrogen in high purity aluminum. Acta Mater 1998;46:6337–49. doi:10.1016/S1359-6454(98)00333-4.

[20] Bhuiyan MS, Toda H, Shimizu K, Su H, Uesugi K, Takeuchi A, et al. The Role of Hydrogen on the Local Fracture Toughness Properties of 7XXX Aluminum Alloys. Metall Mater Trans A 2018. doi:10.1007/s11661-018-4880-0.

[21] Ungár T, Borbély A. The effect of dislocation contrast on x-ray line broadening: A new approach to line profile analysis. Appl Phys Lett 1996;69:3173–5. doi:10.1063/1.117951.

[22] Shirai Y. Behavior of vacancies in aluminum watched by positrons. J Japan Inst Light Met 2006;56:629–34. doi:10.2464/jilm.56.629.

[23] Toda H, Shimizu K, Uesugi K, Suzuki Y, Kobayashi M. Application of Dual-Energy K-Edge Subtraction Imaging to Assessment of Heat Treatments in Al-Cu Alloys. Mater Trans 2010;51:2045–8. doi:10.2320/matertrans.L-M2010819.

[24] Kak AC, Slaney M. Principles of computerized tomographic imaging. Society for Industrial and Applied Mathematics; 2001.

[25] Lorensen WE, Cline HE, Lorensen WE, Cline HE. Marching cubes: A high resolution 3D surface construction algorithm. Proc. 14th Annu. Conf. Comput. Graph. Interact. Tech. - SIGGRAPH '87, vol. 21, New York, New York, USA: ACM Press; 1987, p. 163–9. doi:10.1145/37401.37422.

[26] Shimizu K, Toda H, Uesugi K, Takeuchi A. Local deformation and fracture behavior of high-strength aluminum alloys under hydrogen influence. under review.

[27] Du WS, Cao R, Yan YJ, Tian ZL, Peng Y, Chen JH. Fracture behavior of 9% nickel high-strength steel at various temperatures: Part I. Tensile tests. Mater Sci Eng A 2008;486:611–25. doi:10.1016/J.MSEA.2007.09.057.

[28] Uginasky GM, Skolnick LP, Stiefel SW. Directional Effects in the Stress Corrosion Cracking of an Aluminum Alloy. CORROSION 2013;25:77–86. doi:10.5006/0010-9312-25.2.77.

[29] Young G a., Scully JR. The effects of test temperature, temper, and alloyed copper on the hydrogen-controlled crack growth rate of an Al-Zn-Mg-(Cu) alloy. Metall Mater Trans A 2002;33:1297–1297. doi:10.1007/s11661-002-0233-z.

[30] Bhuiyan MS, Toda H, Peng Z, Hang S, Horikawa K, Uesugi K, et al. Combined microtomography, thermal desorption spectroscopy, X-ray diffraction study of hydrogen trapping behavior in 7XXX aluminum alloys. Mater Sci Eng A 2016;655:221–8. doi:10.1016/j.msea.2015.12.092.

[31] Kirchheim R, Somerday B, Sofronis P. Chemomechanical effects on the separation of interfaces occurring during fracture with emphasis on the hydrogen-iron and hydrogen-nickel system. Acta Mater 2015;99:87–98. doi:10.1016/j.actamat.2015.07.057.

[32] Carling K, Wahnström G, Mattsson TR, Mattsson AE, Sandberg N, Grimvall G. Vacancies in metals: from first-principles calculations to experimental data. Phys Rev Lett 2000;85:3862–5. doi:10.1103/PhysRevLett.85.3862.

[33] Militzer M, Sun WP, Jonas JJ. Modelling the effect of deformation-induced vacancies on segregation and precipitation. Acta Metall Mater 1994;42:133–41. doi:10.1016/0956-7151(94)90056-6.

[34] Deschamps A, Fribourg G, Bréchet Y, Chemin JL, Hutchinson CR. In situ evaluation of dynamic precipitation during plastic straining of an Al–Zn–Mg–Cu alloy. Acta Mater 2012;60:1905–16. doi:10.1016/J.ACTAMAT.2012.01.002.

[35] Witzel W. Vacancy Production by Thermal Jogs during Plastic Deformation. Zeitschrift Fuer Met 1973;64:585–9.

[36] Bendo A, Matsuda K, Lee S, Nishimura K, Toda H, Shimizu K, et al. unpublished work.

[37] Bendo A, Matsuda K, Lee S, Nishimura K, Nunomura N, Toda H, et al. Atomic scale HAADF-STEM study of η′ and η 1 phases in peak-aged Al–Zn–Mg alloys. J Mater Sci 2018;53:4598–611. doi:10.1007/s10853-017-1873-0.

[38] Bendo A, Matsuda K, Lee S, Nishimura K, Toda H, Shimizu K, et al. Microstructure evolution in a hydrogen charged and aged Al–Zn–Mg alloy. Materialia 2018;3:50–6. doi:10.1016/j.mtla.2018.09.035.

[39] Smith SW, Scully JR. The identification of hydrogen trapping states in an Al-Li-Cu-Zr alloy using thermal desorption spectroscopy. Metall Mater Trans A Phys Metall Mater Sci 2000;31:179–93. doi:10.1007/s11661-000-0064-8.

[40] Ebihara K, Yamaguchi M, Tsuru T, Itakura M. Interpretation of thermal desorption spectra of hydrogen from aluminum using numerical simulation. J Japan Inst Light Met 2018;68:596–602. doi:10.2464/jilm.68.596.

[41] Sofronis P, McMeeking RM. Numerical analysis of hydrogen transport near a blunting crack tip. J Mech Phys Solids 1989;37:317–50. doi:10.1016/0022-5096(89)90002-1.

[42] Olden V, Thaulow C, Johnsen R. Modelling of hydrogen diffusion and hydrogen induced cracking in supermartensitic and duplex stainless steels. Mater Des 2008;29:1934–48. doi:10.1016/J.MATDES.2008.04.026.

[43] Toda H, Kamiko T, Tanabe Y, Kobayashi M, Leclere DJ, Uesugi K, et al. Diffraction-amalgamated grain boundary tracking for mapping 3D crystallographic orientation and strain fields during plastic deformation. Acta Mater 2016;107:310–24. doi:10.1016/J.ACTAMAT.2016.01.072.

[44] Csontos AA, Starke EA. The effect of inhomogeneous plastic deformation on the ductility and fracture behavior of age hardenable aluminum alloys. Int J Plast 2005;21:1097–118. doi:10.1016/j.ijplas.2004.03.003.

[45] Neeraj T, Srinivasan R, Li J. Hydrogen embrittlement of ferritic steels: Observations on deformation microstructure, nanoscale dimples and failure by nanovoiding. Acta Mater 2012;60:5160–71. doi:10.1016/j.actamat.2012.06.014.

[46] Martin ML, Fenske J a., Liu GS, Sofronis P, Robertson IM. On the formation and nature of quasi-cleavage fracture surfaces in hydrogen embrittled steels. Acta Mater 2011;59:1601–6. doi:10.1016/j.actamat.2010.11.024.

[47] Zhang Z, Obasis G, Morana R, Preuss M. Acta Materialia Hydrogen assisted crack initiation and propagation in a nickel-based superalloy. Acta Mater 2016;113:272–83. doi:10.1016/j.actamat.2016.05.003.

[48] Deng Y, Barnoush A. Hydrogen embrittlement revealed via novel in situ fracture experiments using notched micro-cantilever specimens. Acta Mater 2018;142:236–47. doi:10.1016/j.actamat.2017.09.057.

[49] De Backer A, Mason DR, Domain C, Nguyen-Manh D, Marinica M-C, Ventelon L, et al. Hydrogen accumulation around dislocation loops and edge dislocations: from atomistic to mesoscopic scales in BCC tungsten. Phys Scr 2017;T170:014073. doi:10.1088/1402-4896/aa9400.

[50] Tien J, Thompson AW, Bernstein IM, Richards RJ. Hydrogen transport by dislocations. Metall Trans A 1976;7:821–9. doi:10.1007/BF02644079.

[51] Dadfarnia M, Martin ML, Nagao A, Sofronis P, Robertson IM. Modeling hydrogen transport by dislocations. J Mech Phys Solids 2015;78:511–25. doi:10.1016/J.JMPS.2015.03.002.

[52] Itoh G, Koyama K, Kanno M. Evidence for the transport of impurity hydrogen with

gliding dislocations in aluminum. Scr Mater 1996;35:695–8. doi:10.1016/1359-6462(96)00200-X.

[53] Itoh G, Jinkoji T, Kanno M, Koyama K. Effect of impurity hydrogen on the deformation and fracture in an Al-5 mass Pct Mg alloy. Metall Mater Trans A 1997;28:2291–5. doi:10.1007/s11661-997-0186-3.

[54] Nagao A, Martin ML, Dadfarnia M, Sofronis P, Robertson IM. The effect of nanosized (Ti,Mo)C precipitates on hydrogen embrittlement of tempered lath martensitic steel. Acta Mater 2014;74:244–54. doi:10.1016/j.actamat.2014.04.051.

[55] Nagao A, Smith CD, Dadfarnia M, Sofronis P, Robertson IM. The role of hydrogen in hydrogen embrittlement fracture of lath martensitic steel 2012. doi:10.1016/j.actamat.2012.06.040.

[56] Nagao A, Dadfarnia M, Somerday BP, Sofronis P, Ritchie RO. Hydrogen-enhanced-plasticity mediated decohesion for hydrogen-induced intergranular and "quasi-cleavage" fracture of lath martensitic steels. J Mech Phys Solids 2018;112:403–30. doi:10.1016/j.jmps.2017.12.016.

[57] Tsuru T, Yamaguchi M, Ebihara K, Itakura M, Shiihara Y, Matsuda K, et al. unpublished work.

[58] Hirayama K, Sek Y, Suzuki T, Toda H, Uesugi K, Takeuchi A, et al. Crystallographic analysis of behavior of hydrogen embrittlement in aluminium alloy using diffraction contrast tomography. Prep n.d.

[59] Su H, Yoshimura T, Toda H, Bhuiyan MS, Uesugi K, Takeuchi A, et al. Influences of Hydrogen Micropores and Intermetallic Particles on Fracture Behaviors of Al-Zn-Mg-Cu Aluminum Alloys. Metall Mater Trans A Phys Metall Mater Sci 2016;47:6077–89. doi:10.1007/s11661-016-3773-3.

[60] Su H, Toda H, Shimizu K, Uesugi K, Takeuchi A, Watanabe Y. Assessment of hydrogen embrittlement via image-based techniques in Al-Zn-Mg-Cu aluminum alloys. Under review.

Table 1 Summary of the microstructural feature of prepared alloys. The six alloys shown this table correspond to alloys in Fig. 2 and alloys denoted as small, medium, and large grain are alloys with the solution treatment time of 0.12, 1.2, and 120ks, respectively.

	Alloys					
	Small grain	Medium grain	Large grain	High C_v - high $\rho_{disl.}$	Low C_v - high $\rho_{disl.}$	Low C_v - low $\rho_{disl.}$
Grain size, d / μm	98	259	678	284	273	372
Dislocation density, $\rho_{disl.}$ / m^{-2}	3.5×10^{14}	5.5×10^{14}	3.1×10^{14}	9.1×10^{15}	8.2×10^{15}	4.7×10^{14}
Volume fraction of pores, V_{pore}	1.5×10^{-4}	9.4×10^{-4}	1.5×10^{-3}	3.4×10^{-5}	2.9×10^{-5}	6.8×10^{-4}
Mean diameter of pores, d_{pore} / μm	2.8	3.3	4.1	2.6	2.5	3.0
Vacancy concentration, $V_{vac.}$	1.5×10^{-9}	1.5×10^{-9}	1.5×10^{-9}	3.5×10^{-3}	1.5×10^{-9}	1.5×10^{-9}
Number density of precipitate, ρ_η / m^{-3}	1.4×10^{23}	1.4×10^{23}	1.4×10^{23}	1.4×10^{23}	1.4×10^{23}	1.4×10^{23}

Table 2 Summary of binding energies derived by first principles simulation.

Trap site	Binding energy, E / kJ·mol^{-1}
Screw dislocation	7.7 [13]
Edge dislocation	16.4 [13]
Grain boundaries	22.2~26.1 [14]
Vacancy	29.0 [15, 16]
Precipitates	7.9~33.9 [17]
Pores (atomic H at surface)	67.5 [18]

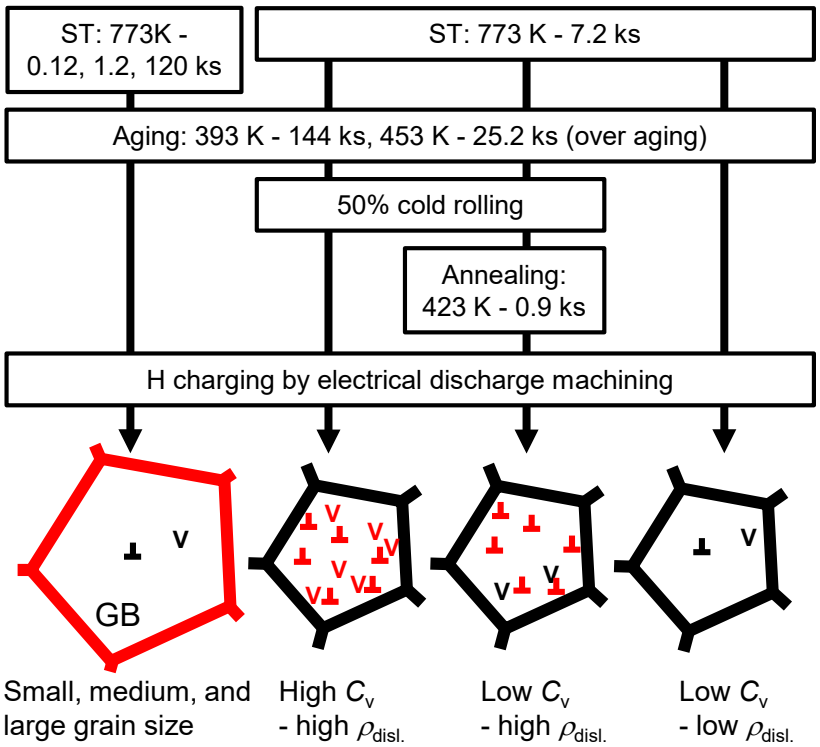

Fig. 1 Schematic illustration of preparation process of specimens used in present research. Grain size, vacancy concentration, C_v, dislocation density, $\rho_{disl.}$, and precipitates were varied by a combination of heat treatments and rolling.

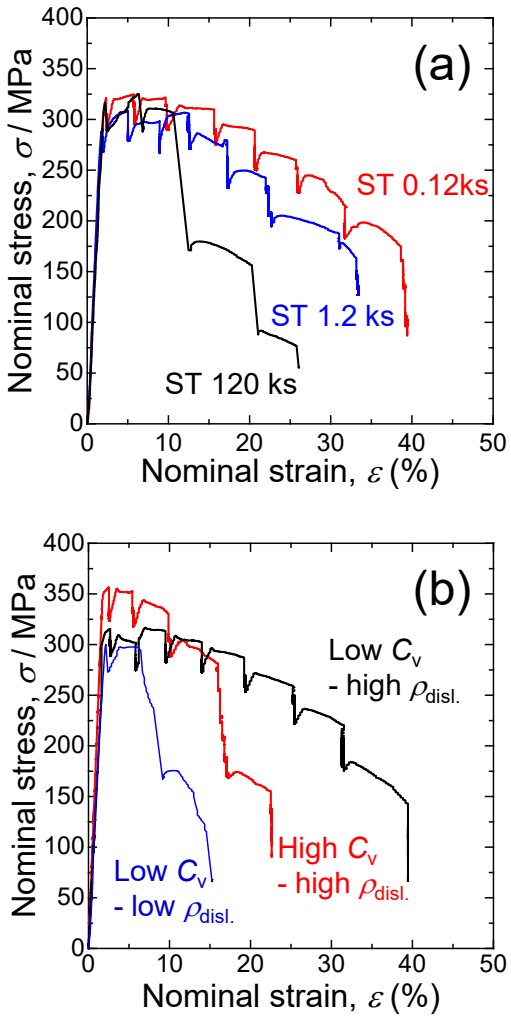

Fig. 2 Nominal stress - nominal strain curves obtained by in situ holding-time tests under synchrotron X-ray tomography: Alloys (a) which performed different times of solution treatment (0.12, 1.2, 120 ks), and (b) which have different C_v and $\rho_{disl.}$ were used.

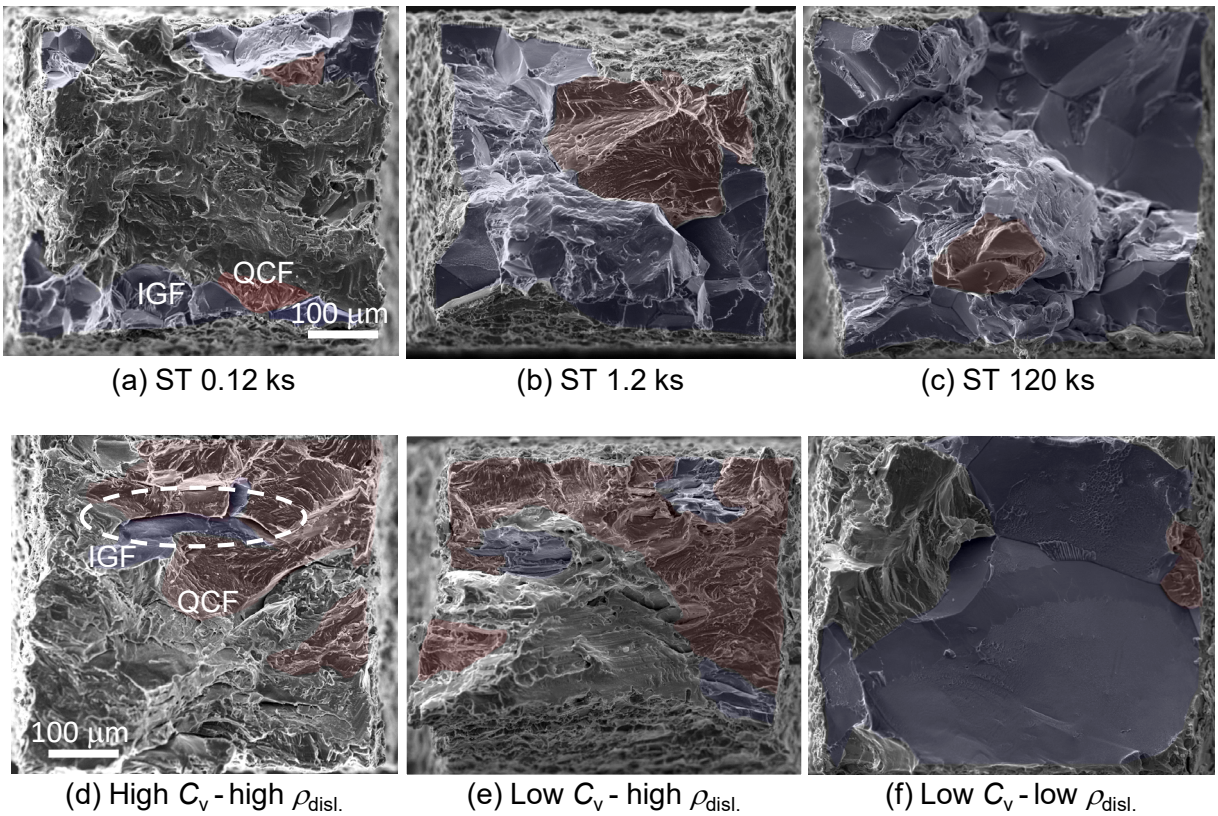

Fig. 3 SEM images of the fracture surface of prepared alloys shown in Fig. 2 after holding-time tests. The region of intergranular fracture (IGF) and quasi-cleavage fracture (QCF) were indicated as blue and red, respectively: (a, b, and c) alloys with time of solution treatment were 0.12, 1.2, and 120 ks, respectively, (d) high C_v – high $\rho_{disl.}$ alloy, (e) low C_v – high $\rho_{disl.}$ alloy (f) low C_v – low $\rho_{disl.}$ alloy.

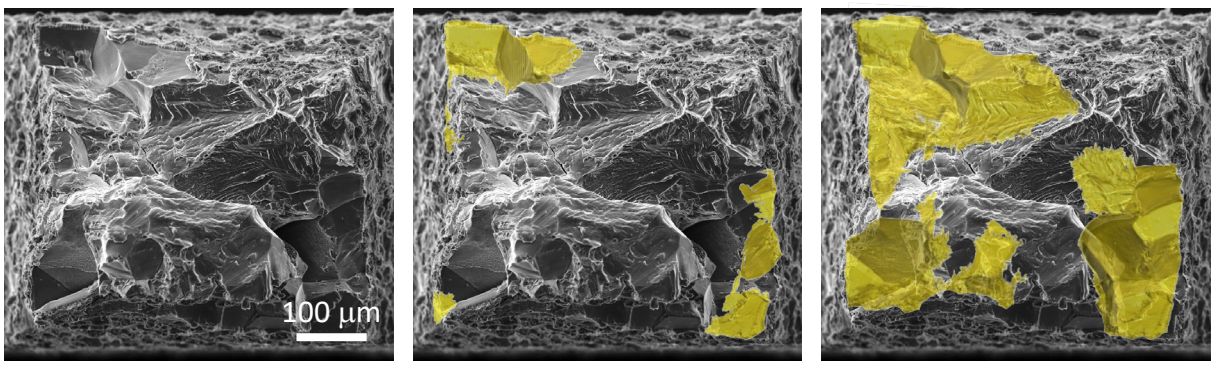

Fig. 4 Visualization of crack growth process captured by synchrotron X-ray tomography. (a) is fracture surface observed from the alloy with time of solution treatment was 1.2 ks, which corresponds to Fig. 3(b). Captured cracks at each strain, indicated as yellow, were superimposed to fracture surface of (a) and shown in (b) and (c).

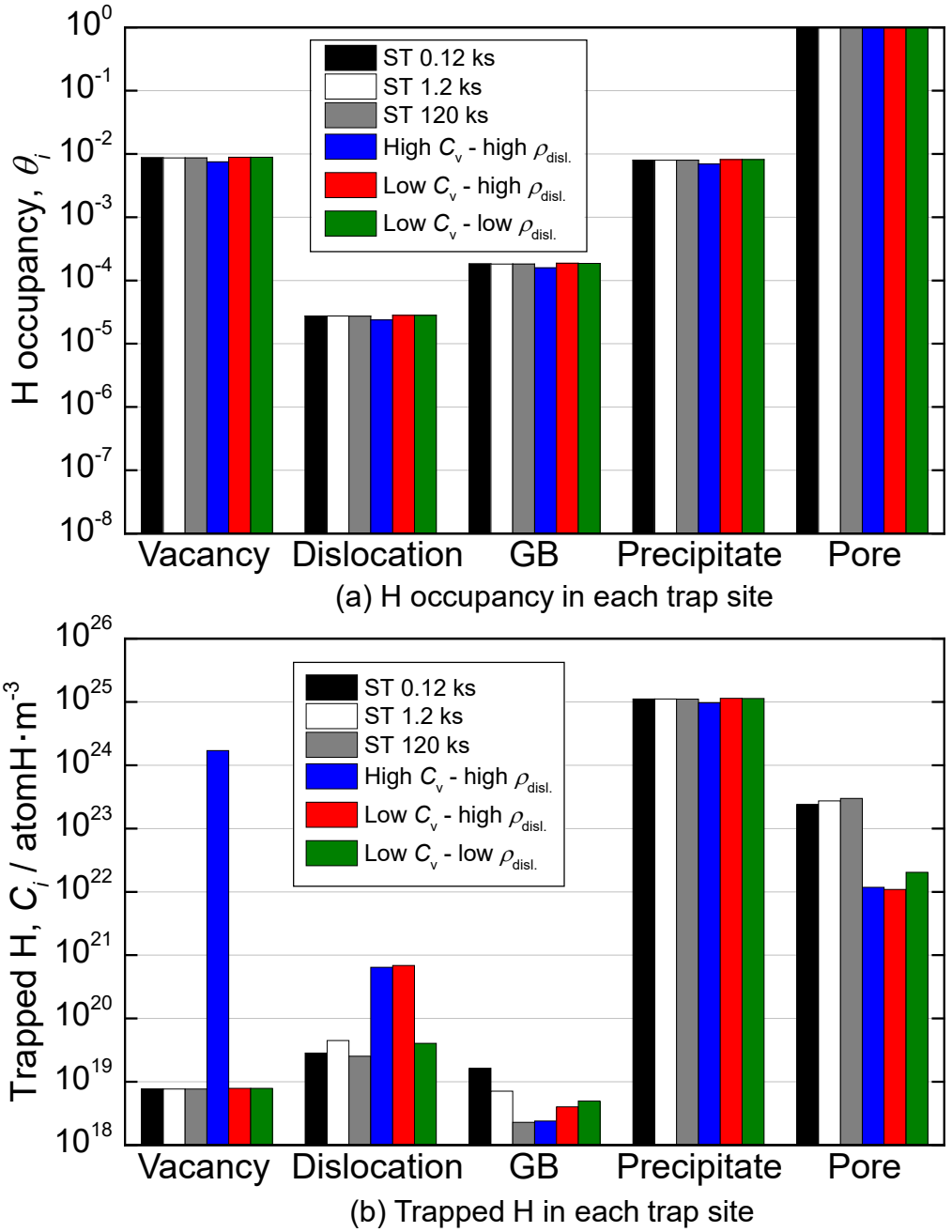

Fig. 5 Summary of the calculation of hydrogen partitioning in prepared alloys. Fig. 5 (a) and (b) indicate hydrogen occupancy and trapped hydrogen content in each site of prepared alloys, respectively.

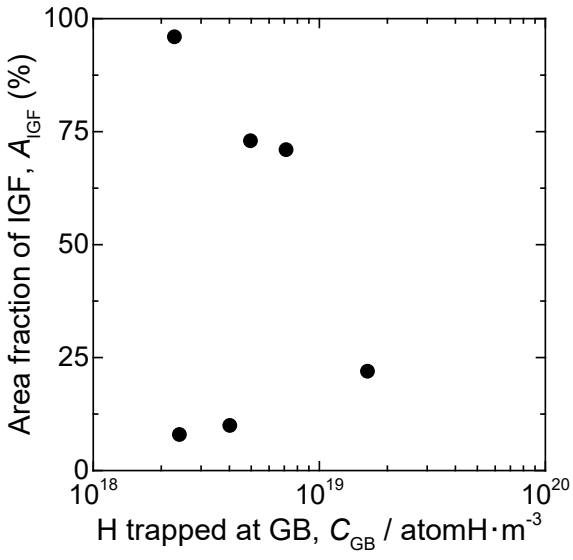

Fig. 6 Relationship between the area fraction of intergranular fracture, A_{IGF}, calculated from Fig. 3 and trapped hydrogen content in grain boundary, C_{GB},which extracted from Fig. 5 (b) in prepared alloys.

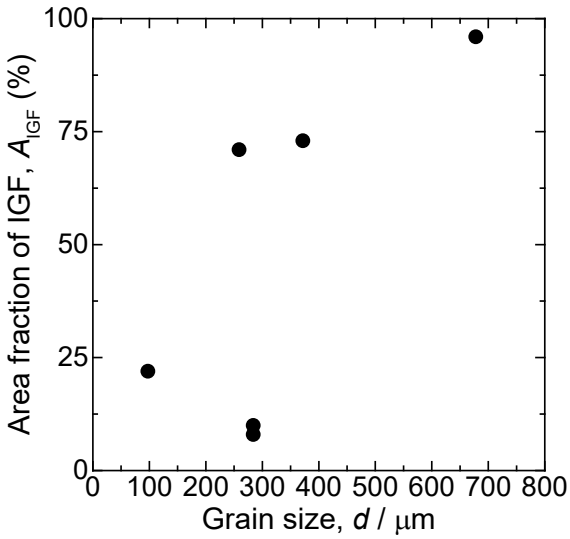

Fig. 7 Relationship between the area fraction of intergranular fracture calculated from Fig. 3 and grain size in prepared alloys.

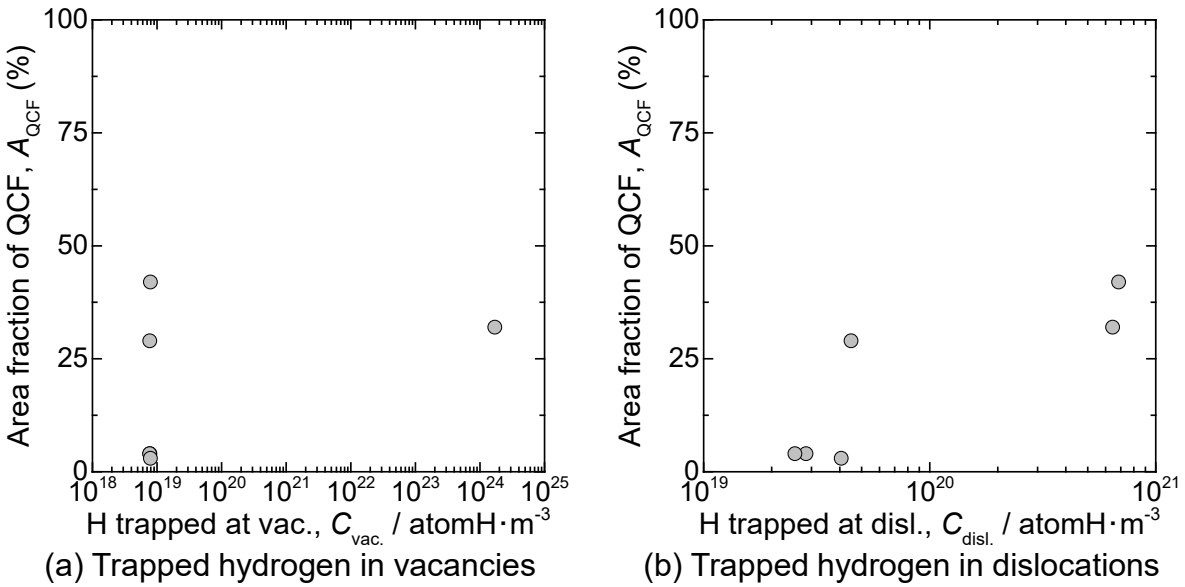

Fig. 8 Relationship between the area fraction of quasi-cleavage fracture, A_{QCF}, calculated from Fig. 3 and trapped hydrogen content in (a) vacancies, $C_{vac.}$, and (b) dislocations, $C_{disl.}$, which extracted from Fig. 5 (b) in prepared alloys.